



Published in final edited form as:

Cell Rep. 2022 August 16; 40(7): 111196. doi:10.1016/j.celrep.2022.111196.

Structural basis for non-canonical integrin engagement by *Bordetella* adenylate cyclase toxin

Jory A. Goldsmith¹, Andrea M. DiVenere², Jennifer A. Maynard^{2,*}, Jason S. McLellan^{1,3,*}

¹Department of Molecular Biosciences, The University of Texas at Austin, Austin, TX 78712, USA

²Department of Chemical Engineering, The University of Texas at Austin, Austin, TX 78712, USA

³Lead contact

SUMMARY

Integrins are ubiquitous cell-surface heterodimers that are exploited by pathogens and toxins, including leukotoxins that target β_2 integrins on phagocytes. The *Bordetella* adenylate cyclase toxin (ACT) uses the $\alpha_M\beta_2$ integrin as a receptor, but the structural basis for integrin binding and neutralization by antibodies is poorly understood. Here, we use cryoelectron microscopy to determine a 2.7 Å resolution structure of an ACT fragment bound to $\alpha_M\beta_2$. This structure reveals that ACT interacts with the headpiece and calf-2 of the α_M subunit in a non-canonical manner specific to bent, inactive $\alpha_M\beta_2$. Neutralizing antibody epitopes map to ACT residues involved in α_M binding, providing the basis for antibody-mediated attachment inhibition. Furthermore, binding to $\alpha_M\beta_2$ positions the essential ACT acylation sites, which are conserved among toxins exported by type I secretion systems, at the cell membrane. These findings reveal a structural mechanism for integrin-mediated attachment and explain antibody-mediated neutralization of ACT intoxication.

In brief

Bordetella adenylate cyclase toxin (ACT) targets leukocytes via surface-expressed integrin $\alpha_M\beta_2$. Goldsmith et al. use cryoelectron microscopy to reveal the structural basis for this non-canonical interaction and show that receptor binding is physically coupled to ACT membrane insertion. This study provides mechanistic insight into ACT function and its integrin-mediated attachment.

Graphical Abstract

This is an open access article under the CC BY license (<http://creativecommons.org/licenses/by/4.0/>).

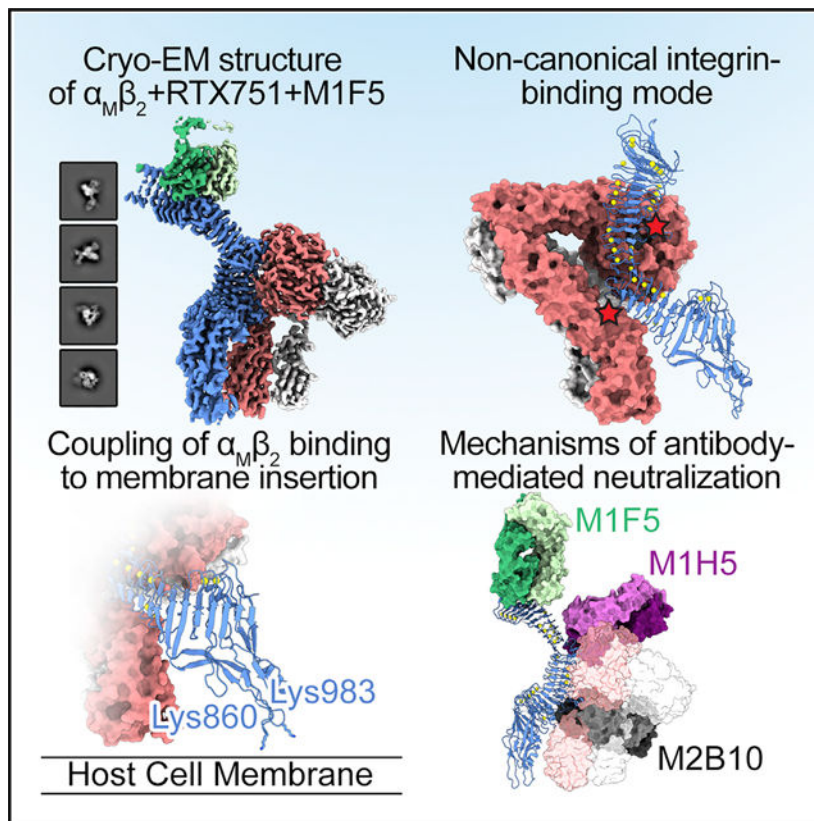
*Correspondence: maynard@che.utexas.edu (J.A.M.), jmclellan@austin.utexas.edu (J.S.M.).

AUTHOR CONTRIBUTIONS

Conceptualization, J.A.G., J.A.M., and J.S.M.; investigation and visualization, J.A.G. and A.M.D., writing – original draft, J.A.G.; writing – review & editing, J.A.G., J.A.M., and J.S.M.; supervision, J.A.M. and J.S.M.

SUPPLEMENTAL INFORMATION

Supplemental information can be found online at <https://doi.org/10.1016/j.celrep.2022.111196>.



INTRODUCTION

Integrins are a family of cell-surface heterodimers that, in animals, mediate cell-cell and cell-extracellular matrix adhesion and serve as receptors for a variety of ligands. Each integrin is made up of one α subunit and one β subunit, and the canonical ligand-binding metal-ion-dependent adhesion site (MIDAS) (Lee et al., 1995b) is within the N-terminal “headpiece.” Integrin activation involves large-scale conformational changes that are coupled to a reorganization of the ligand-binding site (Emsley et al., 2000; Lee et al., 1995a, 1995b; Shimaoka et al., 2003; Takagi et al., 2002). For many integrins, the inactive conformation is the “bent” state, where the integrin headpiece points toward the membrane at an approximately 20° angle relative to the membrane-anchored “tailpiece” (Nishida et al., 2006; Takagi et al., 2002, 2003; Xiong et al., 2001). During activation, a reorganization of the MIDAS allows for high-affinity ligand binding (Emsley et al., 2000; Lee et al., 1995a, 1995b; Shimaoka et al., 2003; Takagi et al., 2002), which is coupled to global conformational changes such as a large hinge motion of the headpiece into the “extended” conformation, as well as separation of the α and β subunit legs and cytoplasmic domains (Nishida et al., 2006; Takagi et al., 2002). Separation of the cytoplasmic domains connects the headpiece state to intracellular signaling (Kim et al., 2003).

Due to their ubiquitous presence on animal cells, integrins are commonly exploited by pathogens to mediate attachment and entry of virulence factors, bacterial cells, and viruses (Hussein et al., 2015; Stewart and Nemerow, 2007; Ulanova et al., 2009). The α_D , α_L , α_M ,

and α_X integrin subunits pair exclusively with β_2 and are expressed on leukocytes (Luo et al., 2007). The pore-forming RTX toxins (Linhartova et al., 2010), a family of related toxins secreted by the bacterial type I secretion system (TISS), contains multiple members that use the β_2 -containing integrins as receptors (Ristow and Welch, 2019). Biochemical data suggest that these toxins interact with β_2 -containing integrins distal to the integrin ligand-binding site, with different toxins binding to different sites (Dileepan et al., 2007; Kieba et al., 2007; Lally et al., 1997; Li et al., 1999; Osicka et al., 2015; Ristow et al., 2019; Ristow and Welch, 2019; Shanthalingam and Srikumaran, 2009). Like all canonical TISS substrates, pore-forming RTX toxins contain a C-terminal RTX domain comprising tandem repeats of a 9-residue calcium-binding motif that adopts a “ β -roll” fold (Baumann et al., 1993; Welch, 1991) and mediates TISS recruitment and secretion (Jarchau et al., 1994; Linhartova et al., 2010; Nicaud et al., 1986; Sebo and Ladant, 1993). Once secreted, the N-terminal portion of pore-forming RTX toxins inserts into target cell membranes and forms pores (Goebel and Hedgpeth, 1982; Linhartova et al., 2010). Pore-forming RTX toxins also contain a pair of conserved lysines that serve as acylation sites (Hackett et al., 1994; Stanley et al., 1994). Addition of an acyl group to at least one of these lysines, which is carried out by an acyltransferase enzyme encoded in the same operon as the toxin and secretion machinery, is essential for activity.

Adenylate cyclase toxin (ACT) from *Bordetella pertussis*, the causative agent of whooping cough, is a member of the pore-forming RTX toxin family (Linhartova et al., 2010). However, unlike other pore-forming RTX toxins, ACT contains an N-terminal adenylate cyclase domain (Figure 1A). ACT inserts into target cells via its pore-forming domain (Figure 1A) and translocates the adenylate cyclase domain across the membrane by a poorly understood mechanism (Vojtova et al., 2006). Once in the host cytosol, activation of the adenylate cyclase by binding to calmodulin results in efficient catalysis that produces aberrantly high levels of cyclic AMP (Wolff et al., 1980). Through this intoxication mechanism, ACT disrupts a variety of leukocyte functions (Confer and Eaton, 1982; Gueirard et al., 1998; Kamanova et al., 2008; Khelef and Guiso, 1995; Pearson et al., 1987; Weingart and Weiss, 2000), promoting *Bordetella* colonization by preventing leukocyte-mediated clearance.

ACT uses the $\alpha_M\beta_2$ integrin as a receptor, with binding required for efficient intoxication of macrophage J774A.1 cells as well as Chinese hamster ovary (CHO) cells recombinantly expressing integrin (Guermonprez et al., 2001; Osicka et al., 2015). The ACT binding site on $\alpha_M\beta_2$ has been shown to include the thigh domain of α_M (Figure 1B), suggesting that ACT engages $\alpha_M\beta_2$ using a non-canonical binding mode (Osicka et al., 2015). ACT was found to intoxicate cells more efficiently when $\alpha_M\beta_2$ was in the inactive conformation (Osicka et al., 2015), but how ACT achieves this conformational specificity is not known. Although the $\alpha_M\beta_2$ -binding site has been localized to within residues 1,166–1,281 of the ACT RTX domain (El-Azami-El-Idrissi et al., 2003), no structural data for the binding of ACT to $\alpha_M\beta_2$ are available, and its mode of non-canonical integrin engagement is poorly understood. In addition, the mechanism by which integrin binding facilitates membrane insertion and intoxication of cells is not known.

Here, we determine a 2.7Å resolution cryoelectron microscopy (cryo-EM) structure of the ACT receptor-binding domain in complex with the $\alpha_M\beta_2$ ectodomain. This structure reveals the basis for non-canonical integrin engagement by ACT, as well as the preference of ACT for the inactive $\alpha_M\beta_2$ conformation. In addition, the structure reveals a relationship between $\alpha_M\beta_2$ binding and insertion of ACT into target cells, with binding positioning the conserved acylation sites at the host-cell membrane. The structure also provides a basis for the antibody-mediated inhibition of ACT, with implications for vaccine development.

RESULTS

$\alpha_M\beta_2$ interacts with RTX751 *in vitro*

As it has been previously suggested that ACT interacts with $\alpha_M\beta_2$ in the bent integrin conformation (Osicka et al., 2015), we purified integrin ectodomains containing an ACID/BASE C-terminal coiled-coil heterodimerization domain, which has been shown to favor the bent conformation in β_2 -containing integrins (Nishida et al., 2006; Xie et al., 2010). To assess whether the $\alpha_M\beta_2$ ectodomain interacts with the purified RTX domain construct RTX751 (ACT residues 751–1,706), we performed surface plasmon resonance (SPR) measurements of $\alpha_M\beta_2$ binding to immobilized RTX751. The $\alpha_M\beta_2$ ectodomain bound to RTX751 with a K_D of 57 nM (Figure 1C), suggesting that the complex was sufficiently stable for cryo-EM studies. Consistent with cell-surface data, transfer of α_M thigh domain residues 597–665 onto $\alpha_X\beta_2$, yielding, $\alpha_X\beta_2(\alpha_M 597–665)$, rescued binding of the $\alpha_X\beta_2$ ectodomain to RTX751 by SPR (Figure 1D). This result confirms that these residues of the α_M thigh domain are important for the interaction of the soluble protein components *in vitro*. However, $\alpha_X\beta_2(\alpha_M 597–665)$ binding to RTX751 exhibited kinetics that deviated from a 1:1 model and exhibited a lower binding level than $\alpha_M\beta_2$ (Figure 1D), which may be due to $\alpha_X\beta_2(\alpha_M 597–665)$ lacking additional α_M residues, partial misfolding of the chimera, or global conformational differences. Lastly, although RTX751 harbors the Lys860 and Lys983 acylation sites (Figure 1A), non-acylated RTX751 was used in this study. This suggests that the acyl modifications are not required for integrin binding.

Cryo-EM structure of RTX751 in complex with $\alpha_M\beta_2$ and M1F5 Fab

To purify the $\alpha_M\beta_2$ +RTX751 complex, we performed anti-RTX751 immunoprecipitation to ensure that all recovered $\alpha_M\beta_2$ heterodimers were in a binding-competent state (Figure 1E). Immunoprecipitation was performed using the M1F5 antibody, as it does not inhibit ACT cell binding or intoxication and would not be expected to affect the RTX- $\alpha_M\beta_2$ interaction (Wang et al., 2015). Binding of the M1F5 Fab to the complex also served to provide additional mass, which can improve cryo-EM particle alignment. SDS-PAGE confirmed that the immunoprecipitated ternary complex of $\alpha_M\beta_2$ +RTX751+M1F5 Fab exhibited the expected 1:1:1 stoichiometry (Figure 1F). The complex was then plunge-frozen on 1.2/1.3 UltrAuFoil grids and a dataset was collected on a Titan Krios using a K3 detector and a 30° stage tilt for 3,831 movies and 0° stage tilt for 500 movies. After motion correction and contrast transfer function estimation, two-dimensional (2D) classification revealed that the particle set contained a mix of the $\alpha_M\beta_2$ +RTX751+M1F5 Fab ternary complex and unbound $\alpha_M\beta_2$. Subsequent 3D classification and heterogeneous refinement allowed us to separate the particles for the ternary complex from those of the unbound $\alpha_M\beta_2$, yielding

final particle sets of 347,508 particles for the ternary complex and 1,114,670 particles for unbound $\alpha_M\beta_2$. Homogeneous refinement of these particle sets resulted in global 2.7 Å maps for each (Figure S1). However, in the global reconstructions for both the ternary complex and unbound $\alpha_M\beta_2$, part of the integrin tailpiece was unresolved. Therefore, we used local refinement with a mask around the tailpiece to obtain maps that were more interpretable in this region (Figure S1). Similarly, the RTX acylation domain (residues 751–1,006) was poorly resolved, so local refinement with a mask around the acylation domain and RTX block I (residues 751–1,055) was performed (Figure S1). The set of global and local reconstructions for both the ternary complex (Figures 2 and S2) and unbound $\alpha_M\beta_2$ (Figure S2) allowed for subsequent model building and refinement.

Docking of the crystal structure of ACT RTX blocks I–III (Goldsmith et al., 2021) into the ternary complex map allowed for unambiguous building of blocks I–IV of the RTX domain, although block V was unresolved (Figure 2). Notably, although the RTX domain in the published structure was in complex with receptor-blocking antibodies M2B10 and M1H5, it superimposes well with blocks I–III of $\alpha_M\beta_2$ -bound RTX751 (main-chain root-mean-square deviation [RMSD] 0.7 Å). This suggests that the RTX domain is rigid and that the $\alpha_M\beta_2$ -binding surface is unaffected by M1F5 binding. The majority of the ACT acylation domain was resolved, but the map contained breaks in the N-terminal ~70 residues that made model building difficult, and therefore a RoseTTaFold-predicted model was used to guide assignment of the register in this region (Baek et al., 2021). Overall, residues 754–1,488 of RTX751 were built, barring one unresolved loop (residues 1,355–1,369). To build the α_M integrin subunit, a crystal structure of $\alpha_X\beta_2$ was used as a starting model (Xie et al., 2010). All of the residues of α_M were built, except for the α_I domain (residues 123–331), which was unresolved due to flexibility relative to the β -propeller and two short unresolved loops in the calf-1 domain.

ACT engages the β -propeller, thigh, and calf-2 domains of α_M via RTX linkers 1 and 2

The cryo-EM structure revealed that ACT forms an extensive interface with $\alpha_M\beta_2$ that primarily involves the RTX domain linker regions between blocks I and II (L1) and between blocks II and III (L2) (Figures 3 and S3). This is consistent with L1 and L2 comprising the epitopes of the two known classes of neutralizing RTX-directed antibodies (Goldsmith et al., 2021; Wang et al., 2015). The $\alpha_M\beta_2$ -binding interface of RTX751 has a surface that is highly complementary to $\alpha_M\beta_2$, resulting in a total buried surface area of 2,938 Å². In contrast to canonical ligands, the RTX domain of ACT engages α_M without involving the ligand-binding α_I domain. Instead, RTX751 inserts into the space between the bent α_M headpiece and tailpiece, and contacts the α_M β -propeller, thigh, and calf-2 domains (Figure 3A). ACT can only contact both the α_M headpiece (containing the β -propeller and thigh domains) and the α_M calf-2 simultaneously if the integrin is bent. This finding provides the structural basis for the specificity of ACT for the bent $\alpha_M\beta_2$ conformation, which was previously hypothesized (Osicka et al., 2015).

The α_M thigh domain is required for binding by RTX751 (Osicka et al., 2015), suggesting it contains a critical portion of the binding interface. Despite most of the thigh domain being too far from RTX751 for contact, the thigh β_2 - β_3 loop extends toward the α_M β -propeller

and interacts with RTX751 L2 (Figure 3A). Arg648 of the thigh $\beta 2$ - $\beta 3$ loop forms a salt bridge with RTX751 Asp1249, a hydrogen bond with RTX751 Ser1244, and π - π stacking interactions on both faces with RTX751 Tyr1227 and Arg1241 (Figure 3A). In addition, Arg646 of the α_M thigh $\beta 2$ - $\beta 3$ loop forms a hydrogen bond with RTX751 Asn1253 and a hydrophobic interaction between its aliphatic region and the RTX751 Tyr1251 side chain (Figure 3A). The extensive contacts formed by these two key arginine residues with RTX751 L2 explain why the thigh $\beta 2$ - $\beta 3$ loop is essential for $\alpha_M\beta_2$ binding (Osicka et al., 2015). In addition, the $\beta 2$ - $\beta 3$ loops of α_X , α_L , and α_D do not contain these arginine residues (Figure 3B), providing a basis for the specificity of ACT for $\alpha_M\beta_2$ and not the other $\beta 2$ -containing integrins (Guermontprez et al., 2001; Osicka et al., 2015).

Aside from the interaction with the α_M thigh $\beta 2$ - $\beta 3$ loop, RTX751 contacts regions of $\alpha_M\beta_2$ that are largely conserved between α_M and α_X (Figure S4A), which likely explains why ACT binding to $\alpha_X\beta_2$ can be rescued upon inclusion of only the α_M thigh domain (Osicka et al., 2015). Within the integrin headpiece, RTX751 contacts the α_M β -propeller domain with L2 as well as with part of RTX block II (Figure 3A). The helix-containing loop in RTX751 L1 also inserts into the space between the α_M β -propeller and calf-2 (Figure 3A). RTX751 forms an interface with the α_M calf-2 domain primarily involving L1 that is largely hydrophobic (Figure 3C). One notable difference between α_M and α_X is that α_M Phe1020, which forms hydrophobic and π - π stacking interactions with RTX751, is a serine in α_X (Ser1017) (Figure S4A). Therefore, the interactions formed by Phe2010 are not critical for ACT binding but may still contribute to the improved binding of $\alpha_M\beta_2$ relative $\alpha_X\beta_2$ (α_M 597–665) (Figure 1D). The ternary complex map also contained a well-resolved N-linked glycan at Asn1059 in α_M calf-2 (Figure 3C), with the core fucose residue of the glycan packing onto RTX751 Leu1124 and Phe1125. Notably, glycans have been shown to be important for ACT binding to $\alpha_M\beta_2$ -expressing cells (Hasan et al., 2015; Morova et al., 2008). Furthermore, investigation of the effects of site-specific glycan mutants showed that ablation of the Asn1059 glycan resulted in a 2-fold decrease in ACT binding, the largest effect among all of the glycans tested (Hasan et al., 2015). However, α_M Asn1059 is substituted for Asp1056 in α_X (Figure S4A), suggesting that this glycan is not strictly required for ACT binding. Overall, these results show that ACT engages $\alpha_M\beta_2$ using a binding mode that differs from typical integrin ligands, whereby an extensive interface is formed with three different domains on the side of the bent α_M subunit.

B. pertussis ACT can efficiently intoxicate J774A.1 murine macrophage cells in a manner that depends on $\alpha_M\beta_2$ binding (Guermontprez et al., 2001; Osicka et al., 2015; Wang et al., 2015), and ACT is essential for lung colonization in infant mouse models of *B. pertussis* infection (Goodwin and Weiss, 1990; Weiss et al., 1984). These data suggest that mouse $\alpha_M\beta_2$ is sufficiently similar to human $\alpha_M\beta_2$ to allow for ACT binding. Analysis of the ACT-binding interface showed that the integrin residues contacting ACT are almost entirely conserved in mouse $\alpha_M\beta_2$. One notable difference is that Arg646 is substituted for Lys646 in the mouse α_M thigh $\beta 2$ - $\beta 3$ loop (Figures 3B and S4B), suggesting that lysine at this position can form similar interactions with RTX751 L2. In addition, just as in α_X , α_M Phe1020 is substituted for a serine in the calf-2 domain of mouse α_M (Ser1021) (Figure S4B). This further corroborates that the hydrophobic and π - π stacking interactions formed by Phe1020 are not strictly required for $\alpha_M\beta_2$ binding by ACT. The only other non-

conserved ACT-binding residue between human and mouse α_M is the substitution of Asn453 for Asp451 in mouse α_M (Figure S4B). However, the aspartate at this position should still form a hydrogen bond with Asn1160 in RTX block II. Thus, the highly conserved ACT-binding interface between human and mouse α_M explains the cross-species reactivity of ACT.

ACT traps a partially extended $\alpha_M\beta_2$ conformation

Previous studies have shown that integrins are flexible in the bent conformation, with multiple copies of $\alpha_X\beta_2$ in the asymmetric unit of a crystal structure exhibiting varying inter-domain angles (Xie et al., 2010). Consistent with these observations, the integrin tailpiece in the cryo-EM reconstruction of unbound $\alpha_M\beta_2$ was poorly resolved (Figure S2B). In contrast, the $\alpha_M\beta_2$ tailpiece was substantially better resolved in the reconstruction of the ternary complex (Figure S2A), likely due to RTX751 stabilizing multiple domains of α_M .

Comparison of unbound $\alpha_M\beta_2$ with RTX751-bound $\alpha_M\beta_2$ showed that the binding of the RTX domain stabilizes a conformation of $\alpha_M\beta_2$ that is partially extended relative to the unbound $\alpha_M\beta_2$ (Figure 4A). RTX751-bound $\alpha_M\beta_2$ is similarly extended relative to the available $\alpha_X\beta_2$ crystal structures (Sen et al., 2013; Xie et al., 2010) (Figure 4B). The bound and unbound $\alpha_M\beta_2$ are related by a hinge motion of the headpiece relative to the tailpiece (Figure 4C). As L2 interacts with the thigh/ β -propeller in the α_M headpiece and L1 interacts with the calf-2 domain in the tailpiece, the rigid RTX domain connecting L1 and L2 stabilizes a fixed distance between the thigh/ β -propeller and calf-2 of α_M . The position of the RTX751 L1 helix between the $\alpha_M\beta_2$ headpiece and tailpiece would result in a steric clash with α_M in the unbound conformation (Figure 4C), meaning the L1 helix may also contribute to the stabilization of the partially extended state. Although the unbound $\alpha_M\beta_2$ adopts a fully bent conformation similar to that observed in bent $\alpha_X\beta_2$ crystal structures (Sen et al., 2013; Xie et al., 2010), the ability of RTX751 to bind $\alpha_M\beta_2$ suggests that it transiently adopts greater headpiece-tailpiece hinge angles in solution, consistent with previous observations (Beglova et al., 2002; Takagi et al., 2002).

$\alpha_M\beta_2$ binding positions the ACT acylation sites at the cell membrane

The structure of RTX751 shows that the acylation domain of RTX toxins is a continuation of the β -roll fold of the RTX domain, with the two acylation sites (Lys860 and Lys983) located at the tips of long loops that protrude from the β -roll core (Figure 5A). Although the acylation sites in ACT are separated by 123 residues, they are positioned at the tips of adjacent loops (Figure 5B). This proximity likely explains the partial redundancy that has been observed between these two sites for ACT (Masin et al., 2005) and suggests that their precise positioning is important for RTX toxin activation. Notably, ACT binding to $\alpha_M\beta_2$ positions Lys860 and Lys983 at the plane of the host-cell membrane, with both side chains pointing toward the membrane (Figure 5A). This suggests that the essential acylations in pore-forming RTX toxins are involved in direct insertion into the target membrane.

The structure also revealed an evolutionary relationship between the conserved acylation domain of pore-forming RTX toxins and linkers 1–4 of *B. pertussis* ACT. We previously observed that the linker regions between RTX blocks of ACT adopt a conserved fold and

contain specific conserved residues, suggesting that they arose through the duplication of a single linker (Goldsmith et al., 2021). The β -roll structure of the acylation domain contains the same higher-order organization as RTX blocks I–V: An RTX block (called block \emptyset) followed by a linker with the conserved fold observed in L1–L4 (Figure 5C). The linker within the acylation domain, called linker 0 or L0, contains Tyr940 at the position of a strictly conserved core-facing tyrosine or phenylalanine (Figure 5D). While L0 contains a glutamine at the position of the conserved glutamate in L1–L4 (Figure 5E), alignment of the *B. pertussis* L0 to L0 from a set of well-studied members of the pore-forming RTX toxin family showed that all other pore-forming RTX toxins analyzed contain the conserved glutamate (Figure S5). Notably, L0 contains a buried lysine side chain (Lys962) that is also present in L1, L2, and L3 (Figure 5F). In all four instances of this buried lysine, the ϵ -amino group occupies the position within the β -roll that typically would contain a calcium ion (Figure 5E). Surprisingly, this lysine is substituted for arginine in the acylation domains of other pore-forming RTX toxins (Figure S5). As the residues surrounding the lysine ϵ -amino group would clash with the guanidinium group of an arginine at this position, the acylation domain of pore-forming RTX toxins with this arginine likely form a bulge to accommodate it. Although the core β sheets of L0–L4 adopt the same fold, the key difference between L0 in the acylation domain and L1–L4 is that L1–L4 contain shorter variable loops and L0 contains a much longer loop harboring the Lys983 acylation site (Figures 5C and S5). The conservation between L0 and L1–L4 suggests that they share a common ancestor. Because L0 is conserved among the pore-forming RTX toxins that generally do not contain the additional linkers seen in ACT, we conclude that L0 is the ancestral linker, and that L1–L4 of ACT arose through the duplication of L0.

Inter-block linkers are immunogenic sites within the ACT RTX domain

M1F5 binds L3 between blocks III and IV (Figure S6), similar to how M2B10 binds L1 and M1H5 binds L2 (Goldsmith et al., 2021). M1F5 forms 2 π - π stacking interactions with L3, 5 hydrogen bonds with L3, 2 π - π stacking interactions with block IV, and 4 hydrogen bonds with block IV (Figure S6A). Thus, all 3 RTX domain antibodies whose epitopes have been mapped by high-resolution structures interact with the RTX linkers (Figure S6B). This suggests that the linkers are particularly immunogenic relative to the RTX blocks.

The ternary complex structure also revealed the basis for ACT neutralization by anti-RTX antibodies M2B10 and M1H5. Consistent with their prevention of $\alpha_M\beta_2$ binding, both M2B10 binding to L1 and M1H5 binding to L2 would result in a steric clash with $\alpha_M\beta_2$ (Figure S6B). By contrast, M1F5 is non-neutralizing as its epitope is not part of the $\alpha_M\beta_2$ -binding interface (Figure S6B). Interestingly, M1H5 mimics Arg648, the key interface residue in the α_M thigh β_2 - β_3 loop (Figure S6C). The guanidinium group of M1H5 CDRH3 Arg98 is in the same position as α_M Arg648, such that they each form a salt bridge with Asp1249, hydrogen bond with Ser1244, and π - π stack with Tyr1227 and Arg1241 in RTX751 L2 (Figure S6C). This suggests that M1H5-like antibodies against ACT may be resistant to escape.

DISCUSSION

Canonical integrin ligands form high-affinity interactions with the MIDAS that involve a specific consensus “RG” tripeptide in the ligand. Many integrin-mediated host-pathogen interactions involve the binding of a pathogen-encoded RGD motif to the integrin MIDAS. In addition, the entry or attachment mechanism often specifically necessitates integrin activation that results from RGD binding to the MIDAS. For example, adenoviruses such as Ad2 and Ad12 use $\alpha_v\beta_5$ and $\alpha_v\beta_3$ as entry receptors (Wickham et al., 1993, 1994). In these viruses, an RGD motif that protrudes from a loop in the penton base of the viral capsid binds to the integrin MIDAS and drives activation and intracellular signaling, with the downstream stimulation of endocytosis facilitating viral entry (Chiu et al., 1999). By contrast, echovirus 1 binds the $\alpha_2\beta_1$ α I domain, but not at the ligand-binding site and in an RGD-independent manner (Jokinen et al., 2010). This RGD-independent binding mode has no preference for the active or inactive conformation and does not drive intracellular signaling. In bacteria, *Yersinia* invasin directly binds to β_1 -containing integrins using an RGD-like motif to mediate cell internalization (Isberg and Leong, 1990; Leong et al., 1995), with *Neisseria meningitidis* NadA likely functioning by a similar mechanism (Nagele et al., 2011). Secreted virulence factors also use integrin receptors, with an RGD motif in the *Helicobacter pylori* T4SS component CagL binding to $\alpha_5\beta_1$, allowing for transport of the T4SS cargo into the host cell (Kwok et al., 2007). Similarly, the staphylococcal toxin LukGH uses an RGD to bind to $\alpha_M\beta_2$, with activation-induced integrin clustering being required for LukGH function (DuMont et al., 2013; Trstenjak et al., 2020).

The structure of RTX751 in complex with $\alpha_M\beta_2$ reveals a structural mechanism by which the inactive integrin conformation can be targeted. Namely, the headpiece and tailpiece of $\alpha_M\beta_2$ must adopt the hinge angle corresponding to the bent integrin conformation to form the full ACT-binding site. Given the importance of the α_M thigh β_2 - β_3 loop for ACT binding, it is conceivable that RTX L2 could bind to the headpiece of extended $\alpha_M\beta_2$ on the host cell surface without forming the interface between L1 and the α_M calf-2. However, receptor-blocking antibodies M2B10 and M1H5 similarly neutralize ACT intoxication of J774A.1 murine macrophages (Wang et al., 2015), even though M2B10 prevents the binding of α_M calf-2 by RTX L1 and is not expected to clash with α_M in the extended conformation. This suggests that $\alpha_M\beta_2$ binding to calf-2 in the bent conformation is required at some point during intoxication.

Hantaviruses have also been shown to preferentially engage the bent $\alpha_v\beta_3$ conformation (Raymond et al., 2005), but the nature of this conformational specificity is unclear. This is because the hantaviral binding site is the PSI domain in the β_2 legs, whose precise arrangement in the extended conformation is not known. The $\alpha_M\beta_2$ -binding mode of ACT suggests that a plausible mechanism of bent specificity for hantaviruses is that it could form additional contacts with the lower integrin legs, or other domains that are only sufficiently close in the bent conformation. Interestingly, a designed disulfide bond that favors hantaviral entry (Raymond et al., 2005) is expected to trap the fully bent $\alpha_v\beta_3$ conformation, with the smallest possible headpiece-tailpiece angle being required for its formation. Such a disulfide bond in $\alpha_M\beta_2$ would likely preclude ACT binding, which requires partial extension relative to the fully bent conformation.

The observation that ACT uses L1 and L2 to engage $\alpha_M\beta_2$ shows that integrin binding evolved independently in ACT, as typical pore-forming RTX toxins that are more similar to *Escherichia coli* HlyA do not contain the RTX linker motif outside of L0 in the acylation domain. HlyA, which uses $\alpha_L\beta_2$ as a receptor (Lally et al., 1997), has a much shorter RTX domain consisting of only the acylation domain (block \emptyset and linker 0), one RTX block, and the C-terminal cap conserved among T1SS substrates (Bumba et al., 2016; Linhartova et al., 2010). However, adapting the inter-block linkers for protein-protein interactions is intuitive as the flat β -roll formed by the calcium-binding repeats is expected to have limited capacity to form a complementary binding surface. Therefore, the absence of inter-block linkers in other pore-forming RTX toxins points to a mystery as to how they bind their integrin receptors. It is possible that some other pore-forming RTX toxins engage β_2 -containing integrins using the N-terminal pore-forming domain. However, swapping the ACT RTX domain for the RTX domain of *E. coli* HlyA altered the specificity of ACT such that it required $\alpha_L\beta_2$ instead of $\alpha_M\beta_2$ on the target cell (Masin et al., 2020). Thus, at least some pore-forming RTX toxins may bind to integrin receptors via RTX domains that lack linker modules. In addition, the conservation of the Lys860 and Lys983 acylation sites and the requirement that they are acylated for toxin function suggest that their mechanistic role is conserved across members of the family. Therefore, it is likely that the convergent mechanisms by which pore-forming RTX toxins bind β_2 -containing integrins also result in their positioning at the membrane. Further structural studies will be required to understand how integrin binding is achieved by other pore-forming RTX toxins.

As the acylation domain contains the conserved linker motif previously observed between RTX blocks I–V (Goldsmith et al., 2021; Motlova et al., 2020), ACT linkers 1–4 likely arose via initial duplication of linker 0. In general, formation of a receptor-binding surface likely provided the selective advantage driving expansion of the ACT RTX domain. However, the ACT receptor-binding site comprises only L1 and L2, and recent work showed that ACT can intoxicate cells as efficiently as wild type when the region of the RTX domain containing L3 and L4 is deleted (Espinosa-Vinals et al., 2021). Therefore, it remains a question as to whether L3 and L4 have any function, potentially involving protein-protein interactions. As the linkers appear to be particularly immunogenic, it is possible that L3 and L4 could bias anti-ACT antibody responses toward non-neutralizing epitopes. In addition, the linker motif in the acylation domain provides a rationale for the observation of impaired membrane insertion and intoxication by ACT containing the mutation Y940A (Masin et al., 2017). This residue is located at the position of the strictly conserved core-facing tyrosine/phenylalanine in the N-terminal portion of the linker motif (Goldsmith et al., 2021). Removal of the phenyl ring by substitution to alanine would therefore be expected to disrupt folding of the linker motif, which could alter the positioning of the Lys983 acylation and preclude efficient membrane insertion. By contrast, the observation that Y940F does not disrupt ACT membrane insertion or intoxication is consistent with the tolerance of the linker motif to either tyrosine or phenylalanine at this position, as exemplified by Phe1486 in L4. A recent study also assessed the effect of alanine substitutions at this position in other pore-forming RTX toxins. Given the importance of this residue in ACT, it is striking that its mutation did not significantly affect the hemolytic activities of *E. coli* HlyA, and only modestly affected *Kingella kingae* RtxA, or *Actinobacillus pleuropneumonia* ApxIA (Lepesheva et al., 2021).

This suggests that the pore-forming RTX toxins more similar to *E. coli* HlyA may have more stable acylation domains than ACT that can maintain the structure of the loop harboring the acylation site homologous to ACT Lys983 despite local unfolding of L0.

In conclusion, we found that ACT achieves specificity for the bent $\alpha_M\beta_2$ conformation by interacting with both the headpiece and tailpiece, which separate during extension. This binding mode differs from other known conformation-specific ligands and monoclonal antibodies and represents a strategy by which pathogens can attach to integrins without favoring activation. Binding to the bent $\alpha_M\beta_2$ conformation also positions the essential acyl groups of ACT at the cell membrane, coupling receptor binding to membrane insertion. These findings will aid in the design of ACT-based reagents that report or induce the bent $\alpha_M\beta_2$ conformation, as well as ACT-based immunogens for next-generation pertussis vaccines.

Limitations of the study

The main limitation of this study is that it only used an *in vitro* reconstituted system to study the binding of the soluble $\alpha_M\beta_2$ ectodomain to RTX751, whereas during the infection of animals, ACT binds membrane-embedded $\alpha_M\beta_2$ on the surface of leukocytes. Therefore, the affinity reported for the interaction of the soluble proteins (57 nM) may not reflect the affinity *in vivo*, where ACT must find $\alpha_M\beta_2$ by sampling a 2D surface. Without the cell or membrane environment, additional structural features of the binding and insertion mechanism may be missed. In addition, the propensity of our $\alpha_M\beta_2$ construct to adopt the bent conformation may affect RTX751 binding, potentially either by improving association due to preventing extension, or inhibiting association by favoring the binding-incompatible fully bent state. The conclusions of this study could also be bolstered further by a systematic mutagenesis-based dissection of individual residue contributions, as well as the optimization of techniques to precisely modulate the integrin conformational state.

STAR★METHODS

RESOURCE AVAILABILITY

Lead contact—Further information and requests for resources and reagents should be directed to and will be fulfilled by the Lead Contact, Jason McLellan
jmclellan@austin.utexas.edu.

Materials availability—All unique/stable reagents generated in this study are available from the Lead Contact with a completed Materials Transfer Agreement.

Data and code availability—Atomic coordinates for $\alpha_M\beta_2$ in complex with RTX751 and M1F5 Fab and for unbound $\alpha_M\beta_2$ have been deposited into the Protein Data Bank and assigned PDB IDs 7USL and 7USM, respectively. Cryo-EM maps for $\alpha_M\beta_2$ in complex with RTX751 and M1F5 Fab have been deposited in the EMDB and assigned codes EMD-26738 (composite map), EMD-27122 (global refinement map), EMD-27123 (tailpiece local refinement map), and EMD-27124 (acylation domain local refinement map). Cryo-EM maps of unbound $\alpha_M\beta_2$ have been deposited in the EMDB and assigned codes EMD-26739

(composite map), EMD-27125 (global refinement map), and EMD-27126 (tailpiece local refinement map).

This paper does not report original code.

Any additional information required to reanalyze the data reported in this paper is available from the Lead Contact upon request.

EXPERIMENTAL MODEL AND SUBJECT DETAILS

FreeStyle 293-F mammalian cells (ThermoFisher) were maintained in FreeStyle 293 expression medium (Gibco) in a 37°C shaker supplied with 8% CO₂ and 80% humidity. These cells were purchased directly from ThermoFisher, and no further authentication was performed.

METHOD DETAILS

Protein expression and purification—A gene encoding RTX751 (ACT residues 751–1706) was cloned into pET22b downstream of an N-terminal 8xHis tag and HRV 3C protease recognition site. This construct was then transformed into *E. coli* BL21 DE3 for protein expression. Cells at OD₆₀₀ = 0.6 were induced with 1 mM IPTG and grown for 16h at 16°C. Following growth, cells were centrifuged for 20 min at 5,000×g. Cells were then resuspended in 50 mM Tris pH 8, 200 mM NaCl, 2 mM CaCl₂, 10 mM imidazole and passed twice through a Microfluidics LM10 microfluidizer at 18,000 psi. Lysate was then centrifuged for 1h at 30,000×g and 4°C. NiNTA resin equilibrated with 50 mM Tris pH 8, 200 mM NaCl, 2 mM CaCl₂, 10 mM imidazole was then magnetically stirred with the soluble fraction for 30 min at 4°C. The resin was then washed on-column with 50 mM Tris pH 8, 200 mM NaCl, 2 mM CaCl₂, 40 mM imidazole. Elution was performed with 50 mM Tris pH 8, 200 mM NaCl, 2 mM CaCl₂, 150 mM imidazole. The elution was then concentrated, run over a Superdex 200 10/300 gel-filtration chromatography column (Cytiva), concentrated, and flash-frozen using liquid N₂ until use.

Genes encoding α_M residues 1–1104 (including native signal sequence), α_X residues 1–1103 (including native signal sequence), or α_X residues 1–1103 (including native signal sequence) with residues 614–682 (595–663 in mature ectodomain) replaced with residues 613–681 (597–665 in mature ectodomain) of α_M , were cloned into p α H upstream of a disulfide bond-forming linker (GCGG) (Xie et al., 2010), an HRV 3C cleavage site (LEVLFQGP), an ACID coiled-coil heterodimerization motif (GENAQCEKELQALEKENAQLEWELQALEKELAQ) (Nishida et al., 2006) and two StrepTagII tags separated by a GlySer linker. A gene encoding β_2 residues 1–699 (including native signal sequence) was cloned into p α H upstream of a disulfide bond-forming linker (DGCG) (Xie et al., 2010) followed by an HRV 3C cleavage site (LEVLFQGP), a BASE coiled-coil heterodimerization motif (GKNAQCCKKLQALKKKNAQLKWKLQALKKKLAQGG) (Nishida et al., 2006) and a 6xHis tag. Plasmid encoding α_M , α_X or $\alpha_X(\alpha_M$ 597–665) ectodomain was transiently co-transfected with plasmid encoding β_2 ectodomain into FreeStyle 293-F cells (Invitrogen) using polyethylenimine (Polysciences). After 6 days, the cell supernatant was harvested and

passed through a 0.22 μm filter. Filtered supernatant was then buffer-exchanged into 20 mM Tris pH 7.5, 150 mM NaCl, 1 mM CaCl_2 , 1 mM MgCl_2 using tangential flow filtration. Integrin heterodimer was then purified from buffer-exchanged supernatant using StrepTactin XT resin equilibrated with 20 mM Tris pH 7.5, 150 mM NaCl, 1 mM CaCl_2 , 1 mM MgCl_2 . Resin was washed with 20 mM Tris pH 7.5, 150 mM NaCl, 1 mM CaCl_2 , 1 mM MgCl_2 and protein was eluted with 20 mM Tris pH 7.5, 150 mM NaCl, 1 mM CaCl_2 , 1 mM MgCl_2 , 50 mM biotin. The elution was then concentrated, run over a Superdex 200 10/300 gel-filtration chromatography column (Cytiva), concentrated, and flash-frozen using liquid N_2 until use.

To express M1F5 IgG, M1H5 IgG, or anti-StrepTagII IgG, plasmid encoding the light chain was transiently co-transfected with plasmid encoding the heavy chain (containing an HRV 3C protease cleavage site in the hinge region) into FreeStyle 293-F cells (Invitrogen) using polyethylenimine (Polysciences). After 6 days, the supernatant was harvested and passed through a 0.22 μm filter. IgG was then purified from filtered supernatant using Protein A Agarose (ThermoFisher). Protein A elutions containing IgG were then dialyzed against 20 mM Tris pH 7.5, 150 mM NaCl, 2 mM CaCl_2 before being flash-frozen using liquid N_2 and stored until use. To generate M1H5 Fab for biolayer interferometry, M1H5 IgG was incubated with 1:20 wt/wt HRV 3C protease overnight at 4°C. Fc was then removed by passing the cleavage reaction over Protein A Agarose (ThermoFisher), after which the Fab was further purified using a Superdex 200 10/300 gel-filtration chromatography column (Cytiva). Fab was then flash-frozen using liquid N_2 and stored until use.

Surface plasmon resonance—For coupling, M1F5 Fab was desalted using a HiPrep 26/10 desalting column (Cytiva) into 10 mM Na-acetate pH 4.0 and concentrated to 1 mg/mL. Using an EDC/NHS amine coupling kit (Cytiva), ~2500 RU M1F5 Fab was coupled onto both flow cells of a CM5 SPR biosensor (Cytiva). Kinetic measurements were performed in a running buffer of 10 mM HEPES pH 7.4, 150 mM NaCl, 1 mM CaCl_2 , 1 mM MgCl_2 , and 0.05% Tween-20. For each cycle of the $\alpha_{\text{M}}\beta_2$ concentration series, ~70 RU RTX751 (10 nM, 5s flow rate, 15s) was coupled onto flow cell 2. Then, buffer (for double-reference subtraction) or $\alpha_{\text{M}}\beta_2$ at 6.13 nM, 12.5 nM, 25 nM, 50 nM, 100 nM, or 200 nM was flowed into both flow cells to measure association for 180s. Dissociation was measured for 600s while flowing in running buffer and data were fit to a global 1:1 binding model for determination of kinetic parameters. For the single-concentration comparison of integrin heterodimer binding ~60 RU RTX751 (10 nM, 5s flow rate, 15s) was coupled onto flow cell 2. Then, buffer (for double-reference subtraction), 200 nM $\alpha_{\text{M}}\beta_2$, 200 nM $\alpha_{\text{X}}\beta_2$ or 200 nM $\alpha_{\text{X}}\beta_2$ (α_{M} 597–665), was flowed into both flow cells to measure association for 180s. Running buffer was subsequently flowed in for 600s to measure dissociation.

$\alpha_{\text{M}}\beta_2$ +RTX751+M1F5 immunoprecipitation—To form a complex of $\alpha_{\text{M}}\beta_2$ +RTX751+M1F5 IgG, 150 μg $\alpha_{\text{M}}\beta_2$, 25 μg RTX751, and 20.6 μg M1F5 IgG (1:1:1 molar ratio of $\alpha_{\text{M}}\beta_2$:RTX751:M1F5 Fab) were mixed in a total volume of 140 μL and allowed to bind at room temperature for 20 min 120 μL of Protein A Agarose (Thermo Fisher) was then equilibrated 3 times in a microcentrifuge tube by mixing with 1 mL 20 mM Tris pH 7.5, 150 mM NaCl, 1 mM CaCl_2 , 1 mM MgCl_2 , centrifuging, and removing the supernatant. The binding reaction was then mixed with the resin, which was subsequently

centrifuged, and the supernatant was removed. To wash the resin, it was mixed with 1.4 mL of 20 mM Tris pH 7.5, 150 mM NaCl, 1 mM CaCl₂, 1 mM MgCl₂, which was then centrifuged and decanted. To elute the ternary complex, 1 µg of HRV 3C protease was added to 120 µL 20 mM Tris pH 7.5, 150 mM NaCl, 1 mM CaCl₂, 1 mM MgCl₂, which was then mixed with the 120 µL resin. The slurry was then rotated overnight at 4°C to ensure homogeneous distribution of the resin and to allow Fab cleavage by HRV 3C. After overnight cleavage, the slurry was centrifuged and the supernatant containing the ternary complex was collected. This procedure was performed in parallel but with buffer instead of RTX751 in the initial binding reaction for the immunoprecipitation negative control.

Cryo-electron microscopy—Immunoprecipitation elution (3 µL) containing α_Mβ₂+RTX751+M1F5 Fab was deposited onto a 1.2/1.3 UltrAuFoil holey gold grid (Electron Microscopy Sciences) that had been plasma cleaned for 4 min using a Gatan Solarus 950 with a 4:1 O₂:H₂ ratio. A Vitrobot Mark IV was used to plunge-freeze the sample, with a blot force of 1, a blot time of 4s, a humidity level of 100%, and at 4°C. Movies were then collected using a K3 detector at a magnification of 22,500× (corresponding to a pixel size of 1.073 Å) in a Titan Krios operating at 300 kV, using 80 e⁻/Å² total dose. Defocus values were varied from -0.8 µm to -2.2 µm. A full description of the data collection parameters can be found in Table S1. Motion correction, CTF estimation, and particle picking were performed in Warp (Tegunov and Cramer, 2019). Particles were subsequently transferred to cryoSPARC v3.2 (Punjani et al., 2017) for 2D classification and 3D reconstruction. The globally refined map as well as the locally refined maps were sharpened using DeepEMhancer (Sanchez-Garcia et al., 2021). Sharpened global and local maps were combined using the Phenix combine_focused_maps function in Phenix (Adams et al., 2002). Model building and refinement were subsequently performed using Coot, Phenix and ISOLDE (Adams et al., 2002; Croll, 2018; Emsley and Cowtan, 2004). Structural biology applications used in this project were compiled and configured by SGrid (Morin et al., 2013).

QUANTIFICATION AND STATISTICAL ANALYSIS

No quantification or statistical tests were performed.

Supplementary Material

Refer to Web version on PubMed Central for supplementary material.

ACKNOWLEDGMENTS

We thank members of the McLellan Laboratory for providing helpful comments on the manuscript. We would like to thank Dr. Sasha Dickinson at the Sauer Structural Biology Laboratory at the University of Texas (UT) at Austin for assistance with cryo-EM data collection. We acknowledge the University of Texas College of Natural Sciences and award RR160023 of the Cancer Prevention and Research Institute of Texas for support of the EM facility at UTexas Austin. This work was funded in part by Welch Foundation grant no. F-0003-19620604 (to J.S.M.) and NIH AI155453 (to J.S.M. and J.A.M.).

REFERENCES

- Adams PD, Grosse-Kunstleve RW, Hung LW, Ioerger TR, McCoy AJ, Moriarty NW, Read RJ, Sacchettini JC, Sauter NK, and Terwilliger TC (2002). PHENIX: building new software for automated crystallographic structure determination. *Acta Crystallogr. D Biol. Crystallogr.* 58, 1948–1954. 10.1107/s0907444902016657. [PubMed: 12393927]
- Afonine PV, Poon BK, Read RJ, Sobolev OV, Terwilliger TC, Urzhumtsev A, and Adams PD (2018). Real-space refinement in PHENIX for cryo-EM and crystallography. *Acta Crystallogr D Struct Biol* 74, 531–544. [PubMed: 29872004]
- Baek M, DiMaio F, Anishchenko I, Dauparas J, Ovchinnikov S, Lee GR, Wang J, Cong Q, Kinch LN, Schaeffer RD, et al. (2021). Accurate prediction of protein structures and interactions using a three-track neural network. *Science* 373, 871–876. 10.1126/science.abj8754. [PubMed: 34282049]
- Baumann U, Wu S, Flaherty KM, and McKay DB (1993). Three-dimensional structure of the alkaline protease of *Pseudomonas aeruginosa*: a two-domain protein with a calcium binding parallel beta roll motif. *EMBO J.* 12, 3357–3364. [PubMed: 8253063]
- Beglova N, Blacklow SC, Takagi J, and Springer TA (2002). Cysteine-rich module structure reveals a fulcrum for integrin rearrangement upon activation. *Nat. Struct. Biol.* 9, 282–287. 10.1038/nsb779. [PubMed: 11896403]
- Bumba L, Masin J, Macek P, Wald T, Motlova L, Bibova I, Klimova N, Bednarova L, Veverka V, Kachala M, et al. (2016). Calcium-driven folding of RTX domain beta-rolls ratchets translocation of RTX proteins through type I secretion ducts. *Mol. Cell* 62, 47–62. 10.1016/j.molcel.2016.03.018. [PubMed: 27058787]
- Chiu CY, Mathias P, Nemerow GR, and Stewart PL (1999). Structure of adenovirus complexed with its internalization receptor, alphavbeta5 integrin. *J. Virol.* 73, 6759–6768. 10.1128/JVI.73.8.6759-6768.1999. [PubMed: 10400774]
- Confer DL, and Eaton JW (1982). Phagocyte impotence caused by an invasive bacterial adenylate cyclase. *Science* 217, 948–950. 10.1126/science.6287574. [PubMed: 6287574]
- Croll TI (2018). ISOLDE: a physically realistic environment for model building into low-resolution electron-density maps. *Acta Crystallogr. D Struct. Biol.* 74, 519–530. 10.1107/S2059798318002425. [PubMed: 29872003]
- Dileepan T, Kannan MS, Walcheck B, and Maheswaran SK (2007). Integrin-EGF-3 domain of bovine CD18 is critical for *Mannheimia haemolytica* leukotoxin species-specific susceptibility. *FEMS Microbiol. Lett.* 274, 67–72. 10.1111/j.1574-6968.2007.00818.x. [PubMed: 17590223]
- DuMont AL, Yoong P, Day CJ, Alonzo F 3rd, McDonald WH, Jennings MP, and Torres VJ (2013). *Staphylococcus aureus* LukAB cytotoxin kills human neutrophils by targeting the CD11b subunit of the integrin Mac-1. *Proc. Natl. Acad. Sci. USA* 110, 10794–10799. 10.1073/pnas.1305121110. [PubMed: 23754403]
- El-Azami-El-Idrissi M, Bauche C, Loucka J, Osicka R, Sebo P, Ladant D, and Leclerc C (2003). Interaction of *Bordetella pertussis* adenylate cyclase with CD11b/CD18: role of toxin acylation and identification of the main integrin interaction domain. *J. Biol. Chem.* 278, 38514–38521. 10.1074/jbc.M304387200. [PubMed: 12885782]
- Emsley J, Knight CG, Farndale RW, Barnes MJ, and Liddington RC (2000). Structural basis of collagen recognition by integrin alpha2beta1. *Cell* 101, 47–56. 10.1016/S0092-8674(00)80622-4. [PubMed: 10778855]
- Emsley P, and Cowtan K (2004). Coot: model-building tools for molecular graphics. *Acta Crystallogr. D Biol. Crystallogr.* 60, 2126–2132. 10.1107/S0907444904019158. [PubMed: 15572765]
- Espinosa-Vinals CA, Masin J, Holubova J, Stanek O, Jurnecka D, Osicka R, Sebo P, and Bumba L (2021). Almost half of the RTX domain is dispensable for complement receptor 3 binding and cell-invasive activity of the adenylate cyclase toxin. *J. Biol. Chem.* 297, 100833. 10.1016/j.jbc.2021.100833. [PubMed: 34051233]
- Goddard TD, Huang CC, Meng EC, Pettersen EF, Couch GS, Morris JH, and Ferrin TE (2018). UCSF ChimeraX: Meeting modern challenges in visualization and analysis. *Protein Sci* 27, 14–25. [PubMed: 28710774]

- Goebel W, and Hedgpeth J (1982). Cloning and functional characterization of the plasmid-encoded hemolysin determinant of *Escherichia coli*. *J. Bacteriol.* 151, 1290–1298. 10.1128/jb.151.3.1290-1298.1982. [PubMed: 7050085]
- Goldsmith JA, DiVenere AM, Maynard JA, and McLellan JS (2021). Structural basis for antibody binding to adenylate cyclase toxin reveals RTX linkers as neutralization-sensitive epitopes. *PLoS Pathog.* 17, e1009920. 10.1371/journal.ppat.1009920. [PubMed: 34547035]
- Goodwin MS, and Weiss AA (1990). Adenylate cyclase toxin is critical for colonization and pertussis toxin is critical for lethal infection by *Bordetella pertussis* in infant mice. *Infect. Immun.* 58, 3445–3447. 10.1128/IAI.58.10.3445-3447.1990. [PubMed: 2401570]
- Gueirard P, Druilhe A, Pretolani M, and Guiso N (1998). Role of adenylate cyclase-hemolysin in alveolar macrophage apoptosis during *Bordetella pertussis* infection in vivo. *Infect. Immun.* 66, 1718–1725. 10.1128/IAI.66.4.1718-1725.1998. [PubMed: 9529102]
- Guermontprez P, Khelef N, Blouin E, Rieu P, Ricciardi-Castagnoli P, Guiso N, Ladant D, and Leclerc C (2001). The adenylate cyclase toxin of *Bordetella pertussis* binds to target cells via the alpha(M)beta(2) integrin (CD11b/CD18). *J. Exp. Med.* 193, 1035–1044. 10.1084/jem.193.9.1035. [PubMed: 11342588]
- Hackett M, Guo L, Shabanowitz J, Hunt DF, and Hewlett EL (1994). Internal lysine palmitoylation in adenylate cyclase toxin from *Bordetella pertussis*. *Science* 266, 433–435. 10.1126/science.7939682. [PubMed: 7939682]
- Hasan S, Osickova A, Bumba L, Novák P, Sebo P, and Osicka R (2015). Interaction of *Bordetella* adenylate cyclase toxin with complement receptor 3 involves multivalent glycan binding. *FEBS Lett.* 589, 374–379. 10.1016/j.febslet.2014.12.023. [PubMed: 25554420]
- Hussein HAM, Walker LR, Abdel-Raouf UM, Desouky SA, Montasser AKM, and Akula SM (2015). Beyond RGD: virus interactions with integrins. *Arch. Virol.* 160, 2669–2681. 10.1007/s00705-015-2579-8. [PubMed: 26321473]
- Isberg RR, and Leong JM (1990). Multiple beta 1 chain integrins are receptors for invasins, a protein that promotes bacterial penetration into mammalian cells. *Cell* 60, 861–871. 10.1016/0092-8674(90)90099-z. [PubMed: 2311122]
- Jarchau T, Chakraborty T, Garcia F, and Goebel W (1994). Selection for transport competence of C-terminal polypeptides derived from *Escherichia coli* hemolysin: the shortest peptide capable of autonomous HlyB/HlyD-dependent secretion comprises the C-terminal 62 amino acids of HlyA. *Mol. Gen. Genet.* 245, 53–60. 10.1007/BF00279750. [PubMed: 7531275]
- Jokinen J, White DJ, Salmela M, Huhtala M, Käpylä J, Sipilä K, Puranen JS, Nissinen L, Kankaanpää P, Marjomäki V, et al. (2010). Molecular mechanism of alpha2beta1 integrin interaction with human echovirus 1. *EMBO J.* 29, 196–208. 10.1038/emboj.2009.326.
- Kamanova J, Kofronova O, Masin J, Genth H, Vojtova J, Linhartova I, Benada O, Just I, and Sebo P (2008). Adenylate cyclase toxin subverts phagocyte function by RhoA inhibition and unproductive ruffling. *J. Immunol.* 181, 5587–5597. 10.4049/jimmunol.181.8.5587. [PubMed: 18832717]
- Khelef N, and Guiso N (1995). Induction of macrophage apoptosis by *Bordetella pertussis* adenylate cyclase-hemolysin. *FEMS Microbiol. Lett.* 134, 27–32. 10.1111/j.1574-6968.1995.tb07909.x. [PubMed: 8593951]
- Kieba IR, Fong KP, Tang HY, Hoffman KE, Speicher DW, Klickstein LB, and Lally ET (2007). *Aggregatibacter actinomycetemcomitans* leukotoxin requires beta-sheets 1 and 2 of the human CD11a beta-propeller for cytotoxicity. *Cell Microbiol.* 9, 2689–2699. 10.1111/j.1462-5822.2007.00989.x. [PubMed: 17587330]
- Kim M, Carman CV, and Springer TA (2003). Bidirectional transmembrane signaling by cytoplasmic domain separation in integrins. *Science* 301, 1720–1725. 10.1126/science.1084174. [PubMed: 14500982]
- Kwok T, Zabler D, Urman S, Rohde M, Hartig R, Wessler S, Misselwitz R, Berger J, Sewald N, König W, and Backert S (2007). *Helicobacter* exploits integrin for type IV secretion and kinase activation. *Nature* 449, 862–866. 10.1038/nature06187. [PubMed: 17943123]
- Lally ET, Kieba IR, Sato A, Green CL, Rosenbloom J, Korostoff J, Wang JF, Shenker BJ, Ortlepp S, Robinson MK, and Billings PC (1997). RTX toxins recognize a beta2 integrin on the surface

- of human target cells. *J. Biol. Chem.* 272, 30463–30469. 10.1074/jbc.272.48.30463. [PubMed: 9374538]
- Lee JO, Bankston LA, Arnaout MA, and Liddington RC (1995a). Two conformations of the integrin A-domain (I-domain): a pathway for activation? *Structure* 3, 1333–1340. 10.1016/s0969-2126(01)00271-4. [PubMed: 8747460]
- Lee JO, Rieu P, Arnaout MA, and Liddington R (1995b). Crystal structure of the A domain from the alpha subunit of integrin CR3 (CD11b/CD18). *Cell* 80, 631–638. 10.1016/0092-8674(95)90517-0. [PubMed: 7867070]
- Leong JM, Morrissey PE, Marra A, and Isberg RR (1995). An aspartate residue of the Yersinia pseudotuberculosis invasin protein that is critical for integrin binding. *EMBO J.* 14, 422–431. [PubMed: 7532130]
- Lepesheva A, Osickova A, Holubova J, Jurnecka D, Knoblochova S, Espinosa-Vinals C, Bumba L, Skopova K, Fiser R, Osicka R, et al. (2021). Different roles of conserved tyrosine residues of the acylated domains in folding and activity of RTX toxins. *Sci. Rep.* 11, 19814. 10.1038/s41598-021-99112-3. [PubMed: 34615931]
- Li J, Clinkenbeard KD, and Ritchey JW (1999). Bovine CD18 identified as a species specific receptor for Pasteurella haemolytica leukotoxin. *Vet. Microbiol.* 67, 91–97. 10.1016/s0378-1135(99)00040-1. [PubMed: 10414364]
- Linhartová I, Bumba L, Mašín J, Basler M, Osi ka R, Kamanová J, Procházková K, Adkins I, Hejnová-Holubová J, Sadílková L, et al. (2010). RTX proteins: a highly diverse family secreted by a common mechanism. *FEMS Microbiol. Rev.* 34, 1076–1112. 10.1111/j.1574-6976.2010.00231.x.
- Luo BH, Carman CV, and Springer TA (2007). Structural basis of integrin regulation and signaling. *Annu. Rev. Immunol.* 25, 619–647. 10.1146/annurev.immunol.25.022106.141618. [PubMed: 17201681]
- Masin J, Basler M, Knapp O, El-Azami-El-Idrissi M, Maier E, Konopasek I, Benz R, Leclerc C, and Sebo P (2005). Acylation of lysine 860 allows tight binding and cytotoxicity of Bordetella adenylate cyclase on CD11b-expressing cells. *Biochemistry* 44, 12759–12766. 10.1021/bi050459b. [PubMed: 16171390]
- Masin J, Osickova A, Jurnecka D, Klimova N, Khaliq H, Sebo P, and Osicka R (2020). Retargeting from the CR3 to the LFA-1 receptor uncovers the adenylyl cyclase enzyme-translocating segment of Bordetella adenylate cyclase toxin. *J. Biol. Chem.* 295, 9349–9365. 10.1074/jbc.RA120.013630. [PubMed: 32393579]
- Masin J, Roderova J, Osickova A, Novak P, Bumba L, Fiser R, Sebo P, and Osicka R (2017). The conserved tyrosine residue 940 plays a key structural role in membrane interaction of Bordetella adenylate cyclase toxin. *Sci. Rep.* 7, 9330. 10.1038/s41598-017-09575-6. [PubMed: 28839199]
- Morin A, Eisenbraun B, Key J, Sanschagrin PC, Timony MA, Ottaviano M, and Sliz P (2013). Collaboration gets the most out of software. *Elife* 2, e01456. 10.7554/eLife.01456. [PubMed: 24040512]
- Morova J, Osicka R, Masin J, and Sebo P (2008). RTX cytotoxins recognize beta2 integrin receptors through N-linked oligosaccharides. *Proc. Natl. Acad. Sci. USA* 105, 5355–5360. 10.1073/pnas.0711400105. [PubMed: 18375764]
- Motlova L, Klimova N, Fiser R, Sebo P, and Bumba L (2020). Continuous assembly of beta-roll structures is implicated in the type I-dependent secretion of large repeat-in-toxins (RTX) proteins. *J. Mol. Biol.* 432, 5696–5710. 10.1016/j.jmb.2020.08.020. [PubMed: 32860773]
- Motulsky HJ, and Brown RE (2006). Detecting outliers when fitting data with nonlinear regression - a new method based on robust nonlinear regression and the false discovery rate. *BMC Bioinformatics* 7, 123. [PubMed: 16526949]
- Nägele V, Heesemann J, Schielke S, Jiménez-Soto LF, Kurzai O, and Ackermann N (2011). Neisseria meningitidis adhesin NadA targets beta1 integrins: functional similarity to Yersinia invasin. *J. Biol. Chem.* 286, 20536–20546. 10.1074/jbc.M110.188326. [PubMed: 21471204]
- Nicaud JM, Mackman N, Gray L, and Holland IB (1986). The C-terminal, 23 kDa peptide of E. coli haemolysin 2001 contains all the information necessary for its secretion by the haemolysin (Hly) export machinery. *FEBS Lett.* 204, 331–335. 10.1016/0014-5793(86)80838-9. [PubMed: 3525227]

- Nishida N, Xie C, Shimaoka M, Cheng Y, Walz T, and Springer TA (2006). Activation of leukocyte beta2 integrins by conversion from bent to extended conformations. *Immunity* 25, 583–594. 10.1016/j.immuni.2006.07.016. [PubMed: 17045822]
- Osicka R, Osickova A, Hasan S, Bumba L, Cerny J, and Sebo P (2015). Bordetella adenylate cyclase toxin is a unique ligand of the integrin complement receptor 3. *Elife* 4, e10766. 10.7554/eLife.10766. [PubMed: 26650353]
- Pearson RD, Symes P, Conboy M, Weiss AA, and Hewlett EL (1987). Inhibition of monocyte oxidative responses by Bordetella pertussis adenylate cyclase toxin. *J. Immunol.* 139, 2749–2754. [PubMed: 2888823]
- Punjani A, Rubinstein JL, Fleet DJ, and Brubaker MA (2017). cryo-SPARC: algorithms for rapid unsupervised cryo-EM structure determination. *Nat. Methods* 14, 290–296. 10.1038/nmeth.4169. [PubMed: 28165473]
- Raymond T, Gorbunova E, Gavrilovskaya IN, and Mackow ER (2005). Pathogenic hantaviruses bind plexin-semaphorin-integrin domains present at the apex of inactive, bent alphavbeta3 integrin conformers. *Proc. Natl. Acad. Sci. USA* 102, 1163–1168. 10.1073/pnas.0406743102. [PubMed: 15657120]
- Ristow LC, Tran V, Schwartz KJ, Pankratz L, Mehle A, Sauer JD, and Welch RA (2019). The extracellular domain of the beta2 integrin beta subunit (CD18) is sufficient for Escherichia coli hemolysin and aggregatibacter actinomycetemcomitans leukotoxin cytotoxic activity. *mBio* 10, e01459–19. 10.1128/mBio.01459-19. [PubMed: 31289186]
- Ristow LC, and Welch RA (2019). RTX toxins ambush immunity’s first cellular responders. *Toxins* 11, E720. 10.3390/toxins11120720. [PubMed: 31835552]
- Sanchez-Garcia R, Gomez-Blanco J, Cuervo A, Carazo JM, Sorzano COS, and Vargas J (2021). DeepEMhancer: a deep learning solution for cryo-EM volume post-processing. *Commun. Biol.* 4, 874. 10.1038/s42003-021-02399-1. [PubMed: 34267316]
- Sebo P, and Ladant D (1993). Repeat sequences in the Bordetella pertussis adenylate cyclase toxin can be recognized as alternative carboxy-proximal secretion signals by the Escherichia coli alpha-haemolysin translocator. *Mol. Microbiol.* 9, 999–1009. 10.1111/j.1365-2958.1993.tb01229.x. [PubMed: 7934926]
- Sen M, Yuki K, and Springer TA (2013). An internal ligand-bound, metastable state of a leukocyte integrin, alphaXbeta2. *J. Cell Biol.* 203, 629–642. 10.1083/jcb.201308083. [PubMed: 24385486]
- Shanthalingam S, and Srikumaran S (2009). Intact signal peptide of CD18, the beta-subunit of beta2-integrins, renders ruminants susceptible to Mannheimia haemolytica leukotoxin. *Proc. Natl. Acad. Sci. USA* 106, 15448–15453. 10.1073/pnas.0906775106. [PubMed: 19706410]
- Shimaoka M, Xiao T, Liu JH, Yang Y, Dong Y, Jun CD, McCormack A, Zhang R, Joachimiak A, Takagi J, et al. (2003). Structures of the alpha L I domain and its complex with ICAM-1 reveal a shape-shifting pathway for integrin regulation. *Cell* 112, 99–111. 10.1016/s0092-8674(02)01257-6. [PubMed: 12526797]
- Stanley P, Packman LC, Koronakis V, and Hughes C (1994). Fatty acylation of two internal lysine residues required for the toxic activity of Escherichia coli hemolysin. *Science* 266, 1992–1996. 10.1126/science.7801126. [PubMed: 7801126]
- Stewart PL, and Nemerow GR (2007). Cell integrins: commonly used receptors for diverse viral pathogens. *Trends Microbiol.* 15, 500–507. 10.1016/j.tim.2007.10.001. [PubMed: 17988871]
- Takagi J, Petre BM, Walz T, and Springer TA (2002). Global conformational rearrangements in integrin extracellular domains in outside-in and inside-out signaling. *Cell* 110, 599–611. 10.1016/s0092-8674(02)00935-2. [PubMed: 12230977]
- Takagi J, Strokovich K, Springer TA, and Walz T (2003). Structure of integrin alpha5beta1 in complex with fibronectin. *EMBO J.* 22, 4607–4615. 10.1093/emboj/cdg445. [PubMed: 12970173]
- Tegunov D, and Cramer P (2019). Real-time cryo-electron microscopy data preprocessing with Warp. *Nat. Methods* 16, 1146–1152. 10.1038/s41592-019-0580-y. [PubMed: 31591575]
- Trstenjak N, Mili D, Graewert MA, Rouha H, Svergun D, Djinovi -Carugo K, Nagy E, and Badarau A (2020). Molecular mechanism of leukocidin GH-integrin CD11b/CD18 recognition and species specificity. *Proc. Natl. Acad. Sci. USA* 117, 317–327. 10.1073/pnas.1913690116. [PubMed: 31852826]

- Ulanova M, Gravelle S, and Barnes R (2009). The role of epithelial integrin receptors in recognition of pulmonary pathogens. *J. Innate Immun.* 1, 4–17. 10.1159/000141865. [PubMed: 20375562]
- Vojtova J, Kamanova J, and Sebo P (2006). Bordetella adenylate cyclase toxin: a swift saboteur of host defense. *Curr. Opin. Microbiol.* 9, 69–75. 10.1016/j.mib.2005.12.011. [PubMed: 16406775]
- Wang X, Gray MC, Hewlett EL, and Maynard JA (2015). The Bordetella adenylate cyclase repeat-in-toxin (RTX) domain is immunodominant and elicits neutralizing antibodies. *J. Biol. Chem.* 290, 23025. 10.1074/jbc.A114.585281. [PubMed: 26386047]
- Weingart CL, and Weiss AA (2000). Bordetella pertussis virulence factors affect phagocytosis by human neutrophils. *Infect. Immun.* 68, 1735–1739. 10.1128/IAI.68.3.1735-1739.2000. [PubMed: 10679000]
- Weiss AA, Hewlett EL, Myers GA, and Falkow S (1984). Pertussis toxin and extracytoplasmic adenylate cyclase as virulence factors of Bordetella pertussis. *J. Infect. Dis.* 150, 219–222. 10.1093/infdis/150.2.219. [PubMed: 6088647]
- Welch RA (1991). Pore-forming cytolysins of gram-negative bacteria. *Mol. Microbiol.* 5, 521–528. 10.1111/j.1365-2958.1991.tb00723.x. [PubMed: 2046545]
- Wickham TJ, Filardo EJ, Cheresh DA, and Nemerow GR (1994). Integrin alpha v beta 5 selectively promotes adenovirus mediated cell membrane permeabilization. *J. Cell Biol.* 127, 257–264. 10.1083/jcb.127.1.257. [PubMed: 7523420]
- Wickham TJ, Mathias P, Cheresh DA, and Nemerow GR (1993). Integrins alpha v beta 3 and alpha v beta 5 promote adenovirus internalization but not virus attachment. *Cell* 73, 309–319. 10.1016/0092-8674(93)90231-e. [PubMed: 8477447]
- Wolff J, Cook GH, Goldhammer AR, and Berkowitz SA (1980). Calmodulin activates prokaryotic adenylate cyclase. *Proc. Natl. Acad. Sci. USA* 77, 3841–3844. 10.1073/pnas.77.7.3841. [PubMed: 6253992]
- Xie C, Zhu J, Chen X, Mi L, Nishida N, and Springer TA (2010). Structure of an integrin with an alpha I domain, complement receptor type 4. *EMBO J.* 29, 666–679. 10.1038/emboj.2009.367. [PubMed: 20033057]
- Xiong JP, Stehle T, Diefenbach B, Zhang R, Dunker R, Scott DL, Joachimiak A, Goodman SL, and Arnaout MA (2001). Crystal structure of the extracellular segment of integrin alpha Vbeta3. *Science* 294, 339–345. 10.1126/science.1064535. [PubMed: 11546839]

Highlights

- Cryo-EM structure of *Bordetella* adenylate cyclase toxin (ACT) bound to integrin $\alpha_M\beta_2$
- ACT interacts with the $\alpha_M\beta_2$ headpiece and tailpiece, preferring the bent conformation
- $\alpha_M\beta_2$ binding positions the ACT acylation sites at the host cell membrane for insertion
- Neutralizing ACT antibodies prevent attachment by sterically clashing with $\alpha_M\beta_2$

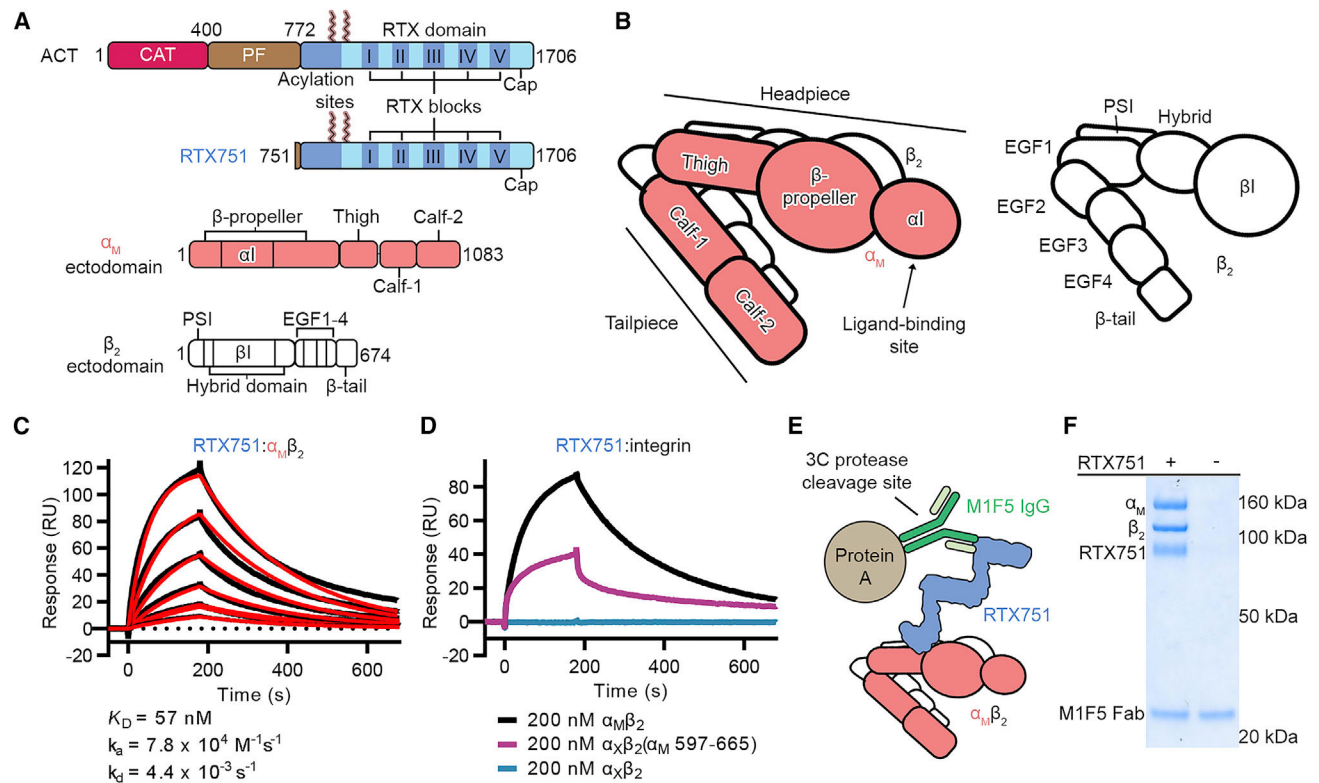


Figure 1. $\alpha_M\beta_2$ interacts with RTX751 *in vitro*

(A) Schematics of ACT and $\alpha_M\beta_2$ protein domains. ACT is the full-length adenylate cyclase toxin secreted by *Bordetella*, and RTX751 is the recombinant C-terminal fragment used in this study. The adenylate cyclase domain is labeled CAT, and the pore-forming domain is labeled PF. Only the ectodomains are shown for α_M and β_2 integrin subunits.

(B) Diagram of the 3D organization of the α_M and β_2 domains. $\alpha_M\beta_2$ is depicted in the bent conformation.

(C) Surface plasmon resonance measurement of RTX751: $\alpha_M\beta_2$ binding kinetics. $\alpha_M\beta_2$ association at varying concentrations was performed for 180 s, with a subsequent dissociation phase of 600 s. The binding data are shown in black, and red traces represent the best fit of the data to a 1:1 binding model. SPR experiments were performed a single time ($N = 1$) with one technical replicate of a single concentration.

(D) Surface plasmon resonance measurements of immobilized RTX751 binding to different integrin constructs at 200 nM. Integrin association was performed for 180 s, with a subsequent dissociation phase of 600 s. Binding data for $\alpha_M\beta_2$ are shown in black, $\alpha_X\beta_2$ in teal, and $\alpha_X\beta_2(\alpha_M 597-665)$ in purple.

(E) Diagram showing the method used for co-immunoprecipitation of the $\alpha_M\beta_2$ -RTX751 complex. The 3C protease site is within the heavy-chain immunoglobulin G (IgG) hinge.

(F) SDS-PAGE of the immunoprecipitation resulting from 3C protease-mediated elution.

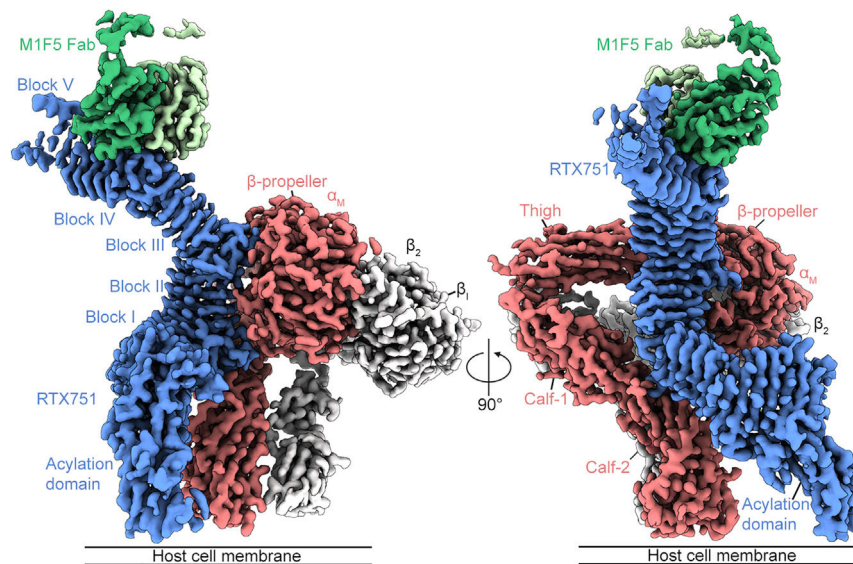


Figure 2. Cryo-EM structure of RTX751 in complex with $\alpha_M\beta_2$ and M1F5 Fab

Cryo-EM reconstruction with the α_M integrin subunit in pink, β_2 integrin subunit in white, RTX751 in blue, M1F5 heavy chain in green, and M1F5 light chain in pale green. This composite map was generated in Phenix (Adams et al., 2002) by combining the reconstructions from the global refinement with those obtained using local refinement for the integrin tailpiece and RTX751 acylation domain. The component maps used to generate the composite were sharpened using DeepEMhancer (Sanchez-Garcia et al., 2021). See also Figures S1 and S2.

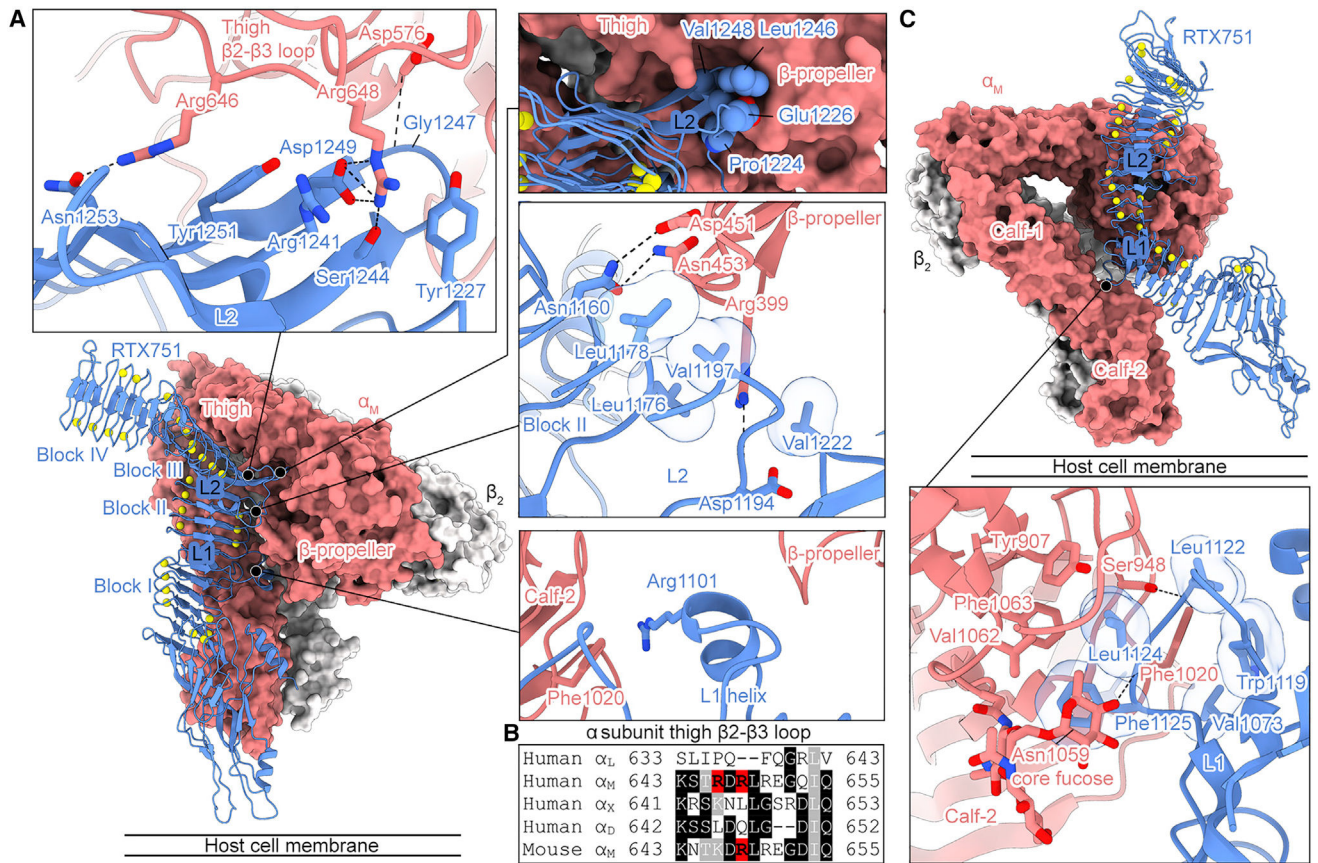


Figure 3. ACT engages α_M using RTX linkers 1 and 2

(A) Model of the RTX751- $\alpha_M\beta_2$ complex. Insets show the interactions formed between α_M and ACT, with interface residues shown as sticks or spheres. Transparent molecular surfaces are shown for RTX751 side chains that form hydrophobic interactions.

(B) Sequence alignment of the thigh β_2 - β_3 loop from all human α integrin subunits that pair with β_2 , as well as mouse α_M . Arg646 and Arg648 in human α_M are highlighted in red.

(C) Interaction between the RTX751 linker 1 (L1) helix and the α_M calf-2 domain. Inset shows the interactions formed between α_M and ACT, with interface residues shown as sticks. Transparent molecular surfaces are shown for RTX751 side chains that form hydrophobic interactions. Oxygen atoms are colored red, nitrogen atoms are blue, and calcium ions are shown as yellow spheres.

See also Figures S3 and S4.

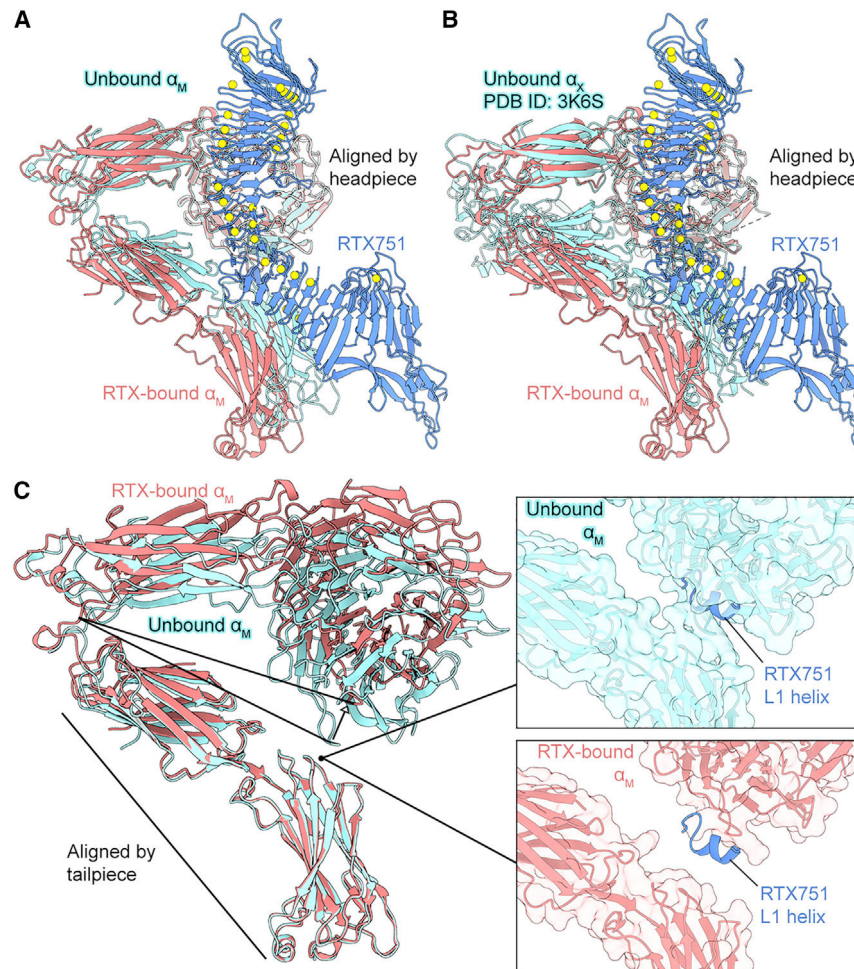


Figure 4. ACT traps a partially extended $\alpha_M\beta_2$ conformation

(A and B) Structure of α_M bound to RTX751 superimposed with either (A) the unbound α_M model derived from the same cryo-EM dataset, or (B) α_X from the crystal structure of $\alpha_X\beta_2$ (PDB: 3K6S) based on alignment of the headpieces. RTX751 is shown in blue, with calcium ions shown as yellow spheres. RTX-bound α_M is colored pink, while unbound α_M or α_X are shown in cyan.

(C) RTX-bound α_M and unbound α_M aligned by the tailpiece to allow visualization of the hinge motion of the headpiece. α_M models are shown as ribbons, along with a transparent molecular surface in the insets. Insets show the position of the RTX751 L1 helix from the RTX751- $\alpha_M\beta_2$ complex as a ribbon.

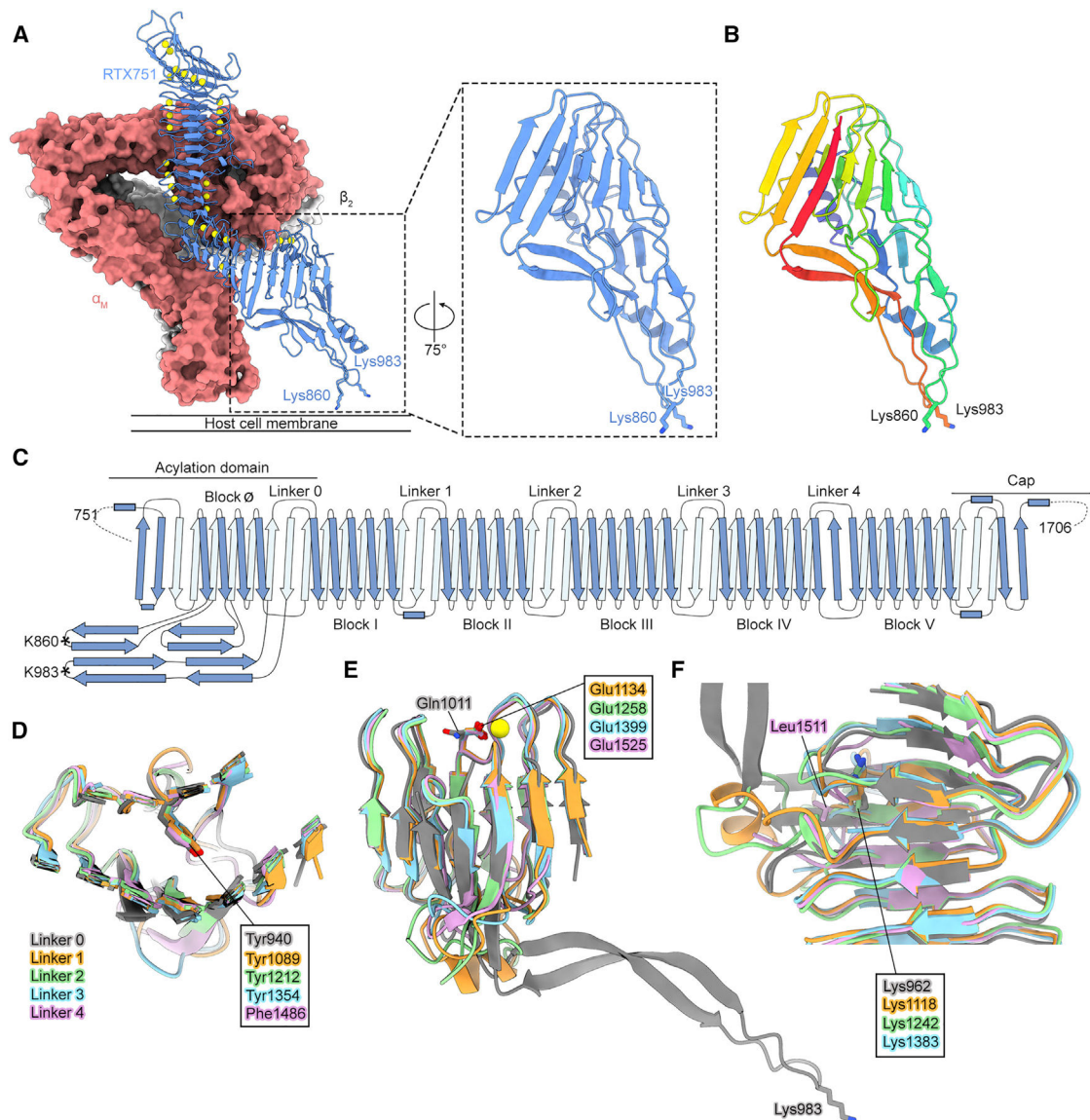


Figure 5. The ACT acylation sites are positioned at the cell membrane

(A) RTX751 in complex with $\alpha_M\beta_2$. Calcium ions are shown as yellow spheres, and the side chains of Lys860 and Lys983 acylation sites are shown as sticks with nitrogen atoms colored dark blue. The approximate location of the host cell membrane is labeled. A zoomed-in view of the acylation domain is shown in the dashed box.

(B) ACT acylation domain with rainbow coloring from blue to red, N to C terminus.

(C) Topology diagram depicting the organization of the ACT RTX domain. β strands are shown as arrows, and α helices are shown as rectangles. β strands on the opposite face of the β -roll are colored pale blue.

(D–F) Structural alignment of the inter-block linkers of the RTX domain. Residues at conserved positions within the linker motif are shown as sticks, with oxygens colored red, nitrogens colored blue, and calcium ions shown as yellow spheres. Residues that conform to the RTX linker consensus motif are labeled in boxes, whereas residues deviating from

the consensus are labeled directly on the residue. (D) Conserved tyrosine/phenylalanine. (E) Conserved glutamate. (F) Conserved internal lysine.
See also Figure S5

Author Manuscript

Author Manuscript

Author Manuscript

Author Manuscript

KEY RESOURCES TABLE

REAGENT or RESOURCE	SOURCE	IDENTIFIER
Antibodies		
Anti-ACT RTX domain antibody, M1F5	This manuscript	N/A
Bacterial and virus strains		
<i>E. coli</i> BL21 (DE3)	New England Biolabs	Cat# C2527H
Chemicals, peptides, and recombinant proteins		
Integrin $\alpha_M\beta_2$ protein	This manuscript	N/A
Integrin $\alpha_X\beta_2$ protein	This manuscript	N/A
Integrin $\alpha_M\beta_2$ (α_M 597–665) protein	This manuscript	N/A
RTX751 protein	This manuscript	N/A
FreeStyle™ 293 Expression Medium	Gibco	Cat# 12338002
OPTI-MEM, Reduced Serum Medium	ThermoFisher	Cat# 11058021
25 kDa linear polyethylenimine	Polysciences	Cat# 3966-2
Deposited data		
CryoEM structure of $\alpha_M\beta_2$ +RTX751+M1F5 Fab	This manuscript	PDB ID: 7USL
$\alpha_M\beta_2$ +RTX751+M1F5 Fab composite EM map	This manuscript	EMDB ID: 26738
$\alpha_M\beta_2$ +RTX751+M1F5 Fab global refinement EM map	This manuscript	EMDB ID: 27122
$\alpha_M\beta_2$ +RTX751+M1F5 Fab tailpiece local EM map	This manuscript	EMDB ID: 27123
$\alpha_M\beta_2$ +RTX751+M1F5 Fab acylation local EM map	This manuscript	EMDB ID: 27124
Cryo-EM structure of $\alpha_M\beta_2$	This manuscript	PDB ID: 7USM
$\alpha_M\beta_2$ composite EM map	This manuscript	EMDB ID: 26739
$\alpha_M\beta_2$ global refinement EM map	This manuscript	EMDB ID: 27125
$\alpha_M\beta_2$ tailpiece local refinement EM map	This manuscript	EMDB ID: 27126
Experimental models: Cell lines		
Freestyle 293-F cells	ThermoFisher Scientific	Cat# R79007
Recombinant DNA		
p α H- α_M	This manuscript	N/A
p α H- α_X	This manuscript	N/A
p α H-(α_M 597–665)	This manuscript	N/A
p α H- β_2	This manuscript	N/A
pET22b-RTX751	This manuscript	N/A
pVRC8400-M1F5_HC	This manuscript	N/A
pVRC8400-M1F5_LC	This manuscript	N/A

REAGENT or RESOURCE	SOURCE	IDENTIFIER
Software and algorithms		
GraphPad Prism	Motulsky and Brown (2006)	V9.0.2
Biacore X100 Evaluation Software	GE Healthcare	V2.0.1
ISOLDE	Croll (2018)	V1.1.0
COOT	Emsley and Cowtan (2004)	http://bernhardcl.github.io/cool/
Phenix	Adams et al. (2002); Afonine et al. (2018)	https://www.phenix-online.org/
ChimeraX	Goddard et al. (2018)	https://www.rbvi.ucsf.edu/chimerax/
cryoSPARC	Punjani et al. (2017)	V2.15.0
Other		
HisPur™ Ni-NTA Resin	ThermoFisher Scientific	Cat# 88223
Pierce™ Protein A Agarose	ThermoFisher Scientific	Cat# 20334
Biacore X100 Sensorchip CM5	Cytiva	Cat# 29149604
EDC/NHS amine coupling kit	Cytiva	Cat# BR100050
Superdex 200 increase 10/300 GL	Cytiva	Cat# 28990944
HiPrep 26/10 desalting	Cytiva	Cat# 17508701
Quantifoil® Holey Gold Film R 1.2/1.3, Gold, 300 mesh	Electron Microscopy Sciences	Cat# Q350AR13A